Urania
Jurnal Ilmiah Daur Bahan Bakar Nuklir

Beranda jurnal: https://ejournal.brin.go.id/urania

THE EFFECT OF TIME IN THE ANODIZING PROCESS ON THE COATING CHARACTERISTICS AND CORROSION BEHAVIOR OF ZIRCONIUM METAL

Manogari Sianturi[1*], Fajar Al Afghani[2], Frisca Ronauli Batubara[3], Sri Rahmadani[4], Romi Saputra[1]
[1]Department of Physics Education, Faculty of Teacher Training and Education, Universitas Kristen Indonesia, Jakarta 13630, Indonesia
[2]Research Center for Nuclear Material and Radioactive Waste Technology – BRIN Kawasan Sains dan Teknologi B.J. Habibie, Bld. 720, Tangerang Selatan, Banten 15314
[3]Department of Physilogy, Faculty of Medicine, Universitas Kristen Indonesia, Jakarta 13630, Indonesia
[4]Mechanical Engineering, Faculty of Engineering, Computer, and Design, Nusa Putra University Sukabumi, Jawa Barat 43152, Indonesia
*e-mail: manogari.sianturi@uki.ac.id

(Submitted: 23–01–2026, Revised: 01–04–2026, Accepted: 06–04–2026)

ABSTRACT

THE EFFECT OF TIME IN THE ANODIZING PROCESS ON THE COATING CHARACTERISTICS AND CORROSION BEHAVIOR OF ZIRCONIUM METAL. Zirconium and its alloys are the standard material for nuclear fuel cladding in Pressurized Water Reactors (PWR) due to their low neutron absorption cross-section, excellent mechanical properties, and good corrosion resistance in high-temperature water. However, the operational environment of a PWR imposes severe conditions that can degrade the cladding integrity over time, including oxidation, hydriding, and mechanical damage such as scratching or denting during fuel refueling operations. These surface defects can act as initiation sites for localized corrosion, potentially compromising the primary containment barrier. This study investigates the effectiveness of electrochemical anodizing as a surface modification technique to enhance the performance of Zirconium. The anodizing process was conducted at a constant voltage of 30 V with varying durations of 10, 15, and 20 minutes. The resulting surface characteristics were evaluated using Optical Microscopy, Digital Microscopy for roughness analysis, and X-Ray Diffraction (XRD). Mechanical reliability was assessed via Vickers Microhardness testing, while Corrosion behavior was studied in a 3.5% NaCl solution using Open Circuit Potential (OCP), Potentiodynamic Polarization (PDP), and Electrochemical Impedance Spectroscopy (EIS). The results demonstrated that increasing the anodizing time significantly improved the surface quality, reducing the arithmetic mean roughness Ra from 0.53 µm (10 min) to 0.24 µm (20 min). XRD analysis confirmed the formation of a crystalline ZrO_2 oxide layer. Electrochemical tests revealed a substantial enhancement in corrosion resistance; the corrosion current density i_{corr} decreased by two orders of magnitude from 12.93 x 10^{-9} A/cm^2 for the substrate to 0.19 x 10^{-9} A/cm^2 for the 20-minute anodized specimen. The study concludes that a 20-minute anodizing treatment at 30 V produces a robust, smooth, and highly corrosion-resistant oxide layer suitable for mitigating degradation in nuclear fuel cladding applications.

Keywords: Zirconium, anodizing, corrosion resistance, cladding, PWR, surface modification.

INTRODUCTION

Zirconium (Zr) and its alloys, such as Zircaloy-4 and Zirlo, are the materials of choice for nuclear fuel cladding in light water reactors (LWR), particularly Pressurized Water Reactors (PWR). This selection is driven by Zirconium's unique combination of properties: an exceptionally low thermal neutron capture cross-section (0.18 barn), which ensures efficient neutron economy, good thermal conductivity, and adequate mechanical strength at elevated temperatures [1, 2]. As the first barrier in the defense-in-depth strategy, the cladding must hermetically seal radioactive fission products preventing their release into the primary coolant.

Despite these advantages, Zirconium cladding faces formidable challenges during its service life. The aggressive operating environment, characterized by high-pressure water (approx. 15.5 MPa) and high temperatures (approx. 300-350°C), promotes waterside corrosion and hydrogen pickup [3, 4]. The oxidation of zirconium ($Zr + 2H_2O \rightarrow ZrO_2 + 2H_2$) not only thins the structural wall but also generates hydrogen, a fraction of which diffuses into the metal matrix, leading to hydride precipitation and embrittlement [5]. Furthermore, beyond steady-state operation, the cladding is subjected to mechanical stress during fuel handling and refueling processes. Physical contact with grid spacers or other assemblies can cause surface scratches, fretting, or dents. These surface imperfections significantly increase local roughness and can serve as stress concentration points or preferential sites for pitting corrosion, accelerating material degradation [6, 7].

Extending the operational life of fuel assemblies and enhanced safety margins, particularly for high-burnup regimes, surface modification techniques have gained attention. The goal is to create a protective surface layer that is harder than the substrate to resist mechanical damage and to be more chemically stable to inhibit corrosion [8]. Among various techniques such as physical vapor deposition (PVD) or laser surface treatment, electrochemical anodizing stands out due to its simplicity, cost-effectiveness, and ability to form a uniform, adherent oxide film (ZrO_2) even on complex geometries [9]. Compared to PVD coatings that are only deposited on top, anodizing on Zr produces a ZrO_2 oxide layer that develops straight from the metal surface, providing significantly stronger adhesion, increased corrosion resistance, and improved thermal stability. Additionally, it creates a consistent, thick, and stable oxide layer that is appropriate for applications requiring long-lasting protection in biological, high-temperature, and harsh environments [1].

Anodizing promotes the growth of a thickened oxide layer that acts as a passivating barrier. While the natural oxide film on Zirconium is protective, it is thin and liable to breakdown. Anodic films, depending on process parameters like voltage, electrolyte, and time, can be engineered to be thicker and more compact [10, 11]. Recent studies have focused on the voltage effects, but the influence of anodizing duration—specifically in the transition from initial film formation to steady-state growth—on the micro-roughness and electrochemical impedance of the surface remains an area for optimization [12]. Limited studies systematically evaluate the effect of anodizing time at fixed voltage on compact oxide growth. Few works correlate roughness evolution, elemental composition, and electrochemical corrosion kinetics simultaneously. There remains a need to evaluate surface stabilization strategies under chloride-containing environments simulating aggressive localized attacks.

This study aims to systematically evaluate the effect of anodizing time (10, 15, and 20 minutes) at a fixed potential of 30 V on the surface characteristics and corrosion behavior of Zirconium. We hypothesize that extending the anodizing duration will not only increase the oxide thickness but also reduce surface roughness through a leveling effect, thereby providing superior corrosion resistance in aggressive chloride environments.

METHODOLOGY

The substrate material used was commercial purity Zirconium metal, cut into coupon specimens with dimensions of 10 mm x 10 mm. The samples were mounted in epoxy resin to expose a single working surface area of 0.5 cm^2. Prior to anodizing, the surfaces were mechanically polished using a sequence of Silicon Carbide (SiC) abrasive papers with grit sizes of 500, 800, 1200, and 2000. This step was crucial to

 DOI: https://doi.org/10.55981/urania.2026.15001

remove the heterogeneous native oxide layer and standardize the initial surface roughness. After polishing, the samples were ultrasonically cleaned in acetone and rinsed with demineralized water to remove any particulate residues.

The anodizing process was carried out in a two-electrode electrochemical cell at room temperature. The Zirconium specimen served as the anode, while a high-purity platinum sheet was used as the cathode to ensure chemical inertness. The electrolyte was a specific aqueous solution tailored for compact film growth (typically phosphate/ammonium based). In the absence of fluoride ions, phosphoric acid electrolytes promote barrier-type compact oxide growth due to limited field-assisted dissolution, preventing nanotubular structure formation [2], [3]. Phosphoric acid (H_3PO_4) at a concentration of 30 g/L is used as the electrolyte for the anodization process. Measuring the phosphoric acid with an analytical balance and combining it with distilled water in a beaker is the first step in the electrolyte production process. When the solution is ready to be employed as an anodizing medium on zirconium metal substrates, it is mixed with a magnetic stirrer until it dissolves uniformly.

A DC power supply was used to apply a constant voltage of 30 V. The anodizing duration varied as the experimental parameter: 10 minutes (Zr-10), 15 minutes (Zr-15), and 20 minutes (Zr-20). Post-anodizing, samples were rinsed and dried in air. A digital multimeter (DMM) was used to monitor the voltage and current during the anodization process. The solution was kept at room temperature to prevent localized heating that would result in non-uniform oxidation. The voltage source was turned off, and the specimen was removed from the electrolyte solution after the anodization period was complete. A hair dryer was used to dry any leftover electrolyte after it had been cleansed with distilled water. All anodized specimens were kept in a closed container, and silica gel was added to regulate the humidity in the storage area prior to testing for corrosion resistance, hardness, and surface morphology examination.

Surface morphology and visual appearance were documented using an Optical Microscope and a high-resolution Digital Microscope. The surface roughness parameters, Arithmetic Mean Roughness (Ra) and Ten-Point Mean Roughness (Rz), were quantified to evaluate the smoothing effect of the treatment. The surface morphology study was supported by microstructural findings. The samples' surface and texture were examined using scanning electron microscopy (SEM) at an accelerating voltage of 15 kV, which provided precise topographical information on the zirconium dioxide (ZrO_2) layer. Porosity, fractures, oxide layer thickness, and surface features that matched each time variation were observed using SEM examination. Additionally, the elemental composition of the coating was determined using Energy Dispersive Spectroscopy (EDS), with a focus on the distribution of phosphorus and oxygen to validate the creation of the ZrO_2 layer and potential interactions with the H_3PO_4 electrolyte. For additional examination, elemental mapping and spectra were both obtained.

The following explanation and reactions have been incorporated:

Zirconium is oxidized under the applied electric field:

$$Zr \rightarrow Zr^{4+} + 4e- \quad (1)$$

Simultaneously, oxygen-containing species (O^{2-} or OH^- derived from water) migrate inward and react with zirconium ions:

$$Zr^{4+} + 2O^{2-} \rightarrow ZrO_2 \quad (2)$$

Alternatively, expressed via water-assisted oxidation:

$$Zr + 2H_2O \rightarrow ZrO_2 + 4H^+ + 4e^- \quad (3)$$

In phosphoric acid electrolyte, the dominant species include:

$$H_3PO_4 \rightleftharpoons H_2PO_4- \rightleftharpoons HPO_4^{2-} \rightleftharpoons PO_4^{3-} \quad (4)$$

Under the strong electric field across the growing oxide film. Negatively charged phosphate ions migrate toward the anode. A fraction of these anions becomes incorporated into the outer oxide region. The incorporation process can be represented schematically as:

$$ZrO_2 + xPO_4^{3-} \rightarrow ZrO_2(PO_4)x \quad (5)$$

The crystalline structure of the anodic oxide layers was analyzed using X-Ray Diffraction (XRD) with Cu-Kα radiation. To assess the resistance to mechanical damage, Vickers Microhardness testing was

performed using a load of 300 gf with a dwell time of 15 seconds; five indentations were made per sample to obtain an average value.

Corrosion performance was evaluated in a 3.5% NaCl solution, chosen to simulate an aggressive corrosive environment that accelerates pitting attack. A standard three-electrode cell was employed, consisting of the Zr specimen (working electrode), an Ag/AgCl reference electrode, and a graphite counter electrode. The measurements were conducted using a Potentiostat/Galvanostat with the following sequence:

1. Open Circuit Potential (OCP): Monitored for 3600 seconds until a stable potential was reached.
2. Potentiodynamic Polarization (PDP): Scanned from -250 mV to +250 mV relative to OCP at a scan rate of 1 mV/s to determine Tafel parameters E_{corr} and i_{corr}.
3. Electrochemical Impedance Spectroscopy (EIS): Conducted at OCP with a sinusoidal perturbation of 10 mV amplitude over a frequency range of 100 kHz to 0.01 Hz.

RESULTS AND DISCUSSION

Surface Morphology and Roughness Analysis

Visual inspection of the samples immediately after anodizing revealed a distinct coloration of the surface. As shown in Figure 1, the surface color shifted from the metallic silver of the substrate to uniform hues of gold and blue. This phenomenon is attributed to the interference of light within the transparent anodic oxide film (ZrO_2), where the perceived color is directly related to the film thickness governed by the anodizing duration [13].

Microstructural analysis via optical microscopy (Figure 2) and SEM (Figure 3) indicated a significant improvement in surface texture. The non-anodized substrate exhibited polishing lines and surface irregularities. However, post-anodizing, these features were progressively smoothed.

The anodization of Zr metal at 10 minutes produced a comparatively uneven surface morphology in Figure 2a. A coating of zirconium oxide had developed at that point, although it was not yet uniformly distributed. The 3D profile data (Figure 2b) revealed that the oxide layer was still in its early phases of formation, resulting in a very rough surface roughness. The duration of anodization was extended to 15 minutes (Figure 2c). Compared to Zr-10, the resulting zirconium oxide layer became more homogeneous, thick, and continuous. This result was also confirmed from the 3D profile of Figure 2d. Figure 2e shows the anodization of Zr metal with a process time of 20 minutes. Increasing the anodization time contributed to the growth and stability of the zirconium oxide layer formed on the metal surface. The layer was more uniform, dense, and surface defects were significantly reduced. The relevant results are confirmed by Figure 2f.

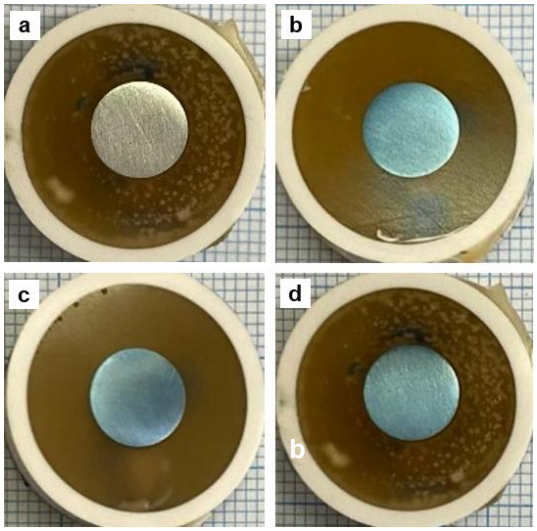

Figure 1. Color of zirconium oxide with various anodizing time of a) Zr, b) Zr-10, c) Zr-15, and d) Zr-20 minutes.

Quantitative roughness data presented in Table 1 and Figure 2 (b,d,f) confirm this observation. The average roughness (Ra) decreased from 0.53 μm for the Zr-10 specimen to 0.34 μm for Zr-15, and finally to 0.24 μm for Zr-20. This trend suggests a "leveling mechanism" where the oxide grows preferentially in the microscopic valleys of the metal surface, effectively reducing the peak-to-valley height [14]. A smoother surface is highly advantageous for nuclear cladding as it reduces the friction coefficient during fuel rod insertion and minimizes the surface area available for corrosive attack.

 DOI: https://doi.org/10.55981/urania.2026.15001

Table 1. Quantitative roughness data of anodized-Zr.

Specimen	Surface Roughness	
	Ra	Rz
Zr-10	0.53	4.35
Zr-15	0.34	4.98
Zr-20	0.24	2.34

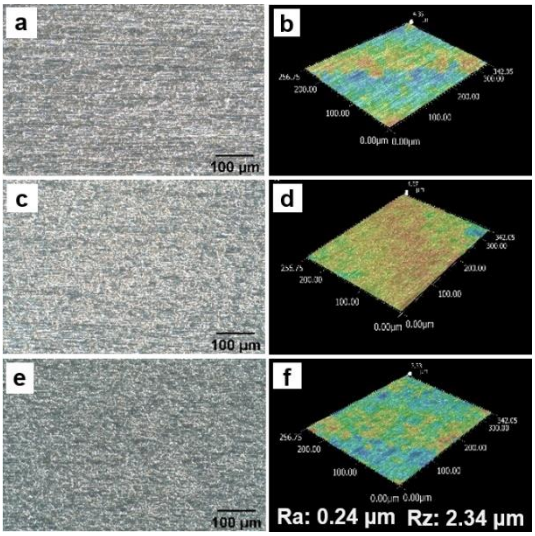

Figure 2. Microstructural analysis via optical microscopy (a,c,e), 3D profile (b,d,f), and surface roughness value (g) of (a,b) Zr-anodized 10 minutes, (c,d) Zr-anodized 15 minutes, and (e,f) Zr-anodized 20 minutes.

The zirconium substrate, whose composition decreased as the anodization duration increased, provided the Zr element. The O element showed that an oxide layer had formed during the anodization processes. The composition of the O element increased as the anodization duration increased, indicating the thickening and expansion of the zirconium oxide layer (ZrO_2). The increase in the O element was formed from 44.66 at% for the Zr-10 specimen, 53.12 at% for the Zr-15 specimen, and the highest for the Zr-20 specimen, namely 54.33 at%. The P element was also found throughout the layer's surface in addition to these primary components. The phosphate-based electrolyte used during the anodizing process is the source of the phosphorus, which is present in trace levels (around 1-2 at%) but is dispersed rather uniformly.

Figure 3 shows SEM images and the corresponding EDS area mapping of zirconium anodized under different duration processes. The surfaces of all the specimens were quite homogeneous and devoid of significant cracks. Increasing the anodization time prevented any significant morphological changes at the micrometer scale. For every modification in anodization time, the elemental mapping findings on the zirconium oxide layer's surface revealed an equitable distribution of elements. The anodized metal surface was dominated by Zr and O elements as shown in Figure 4.

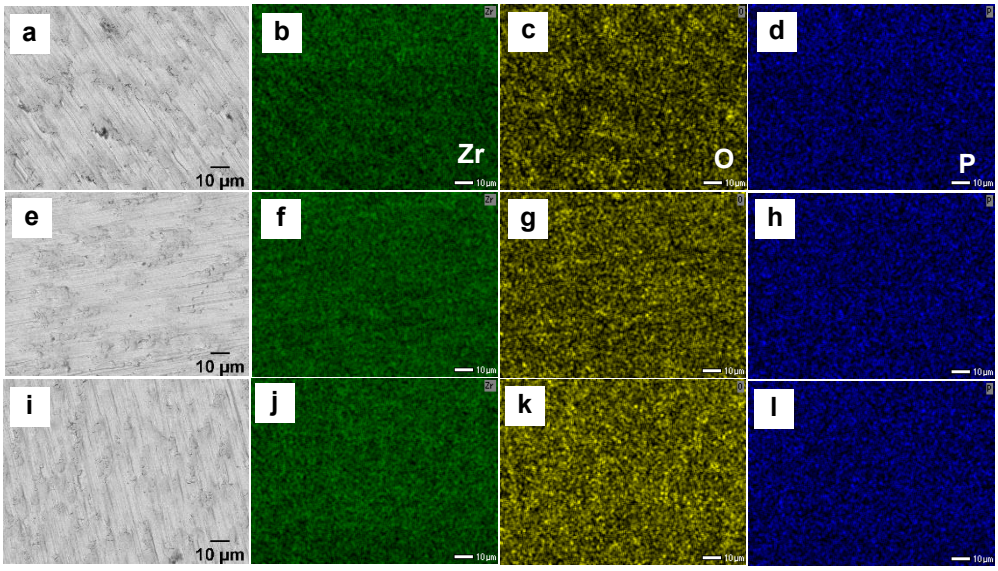

Figure 3. Surface view SEM images and the corresponding EDS area mapping of zirconium anodized of (a-d) Zr-10, (e-h) Zr-15, and (i-l) Zr-20 minutes.

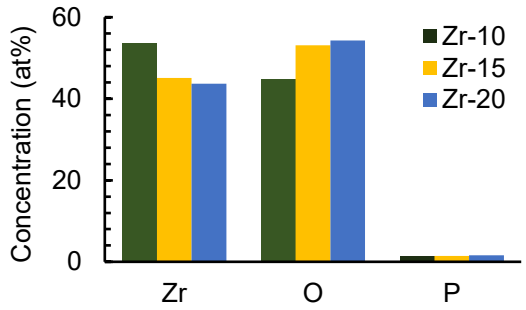

Figure 4. Elemental mapping of zirconium anodized by EDS.

Phosphorus detected in the anodic film originates from field-assisted incorporation of phosphate species during anodization rather than residual electrolyte contamination. The concentration remains low and relatively independent of anodizing time, indicating incorporation primarily during early barrier layer formation. At the detected level (~1–2 at%), phosphorus is not expected to adversely affect zirconium cladding performance, although high-temperature reactor-condition validation remains necessary

Crystalline Structure and Microhardness the XRD patterns shown in Figure 5 display sharp diffraction peaks corresponding to Zirconium Oxide (ZrO_2). The analysis suggests the presence of most tetragonal crystalline phase CDD / PDF card: 00-050-1089, which is notable as anodic films formed at lower voltages are often amorphous. The formation of this crystalline phase contributes to the chemical stability of the coating [15]. Diffraction peaks for the zirconium (Zr) and zirconium oxide (ZrO_2) phases were detected on all anodized specimens. The ZrO_2 peak's formation indicates that the anodization procedure was effective in generating an oxide layer on the zirconium substrate's surface. The ZrO_2 diffraction peak's clarity tended to rise with increasing anodization time, especially in the Zr-20 specimen, which showed the maximum peak intensity. This suggests that extended anodization durations encourage the formation of an oxide layer that is thicker and/or more crystalline. In the meantime, peaks from the Zr phase were still identified, suggesting that the relatively tiny oxide layer thickness allowed X-rays to proceed toward the substrate. In general, the XRD data confirm that different anodization times affect the zirconium oxide layer's growth and crystal properties. At the anode, the reaction that occurs can be written as:

$$Zr \rightarrow Zr^{4+} + 4e^{-} \quad (6)$$

$$Zr^{4+} + 2\,O^{2-} \rightarrow ZrO_2 \quad (7)$$

Meanwhile, at the cathode a reduction reaction takes place, usually involving the evolution of hydrogen gas:

$$4\,H^{+} + 4\,e^{-} \rightarrow 2\,H_2 \quad (8)$$

Mechanical integrity was evaluated via Vickers microhardness (HV). As detailed in Table 2, the hardness values were relatively stable across the anodized samples: 144.41±8.99 HV (10 min), 144.66±7.84 HV (15 min), and 142.88±6.96 HV (20 min). Although the macroscopic hardness did not show a drastic increase compared to the substrate (likely due to the indentation depth exceeding the thin oxide layer thickness), the presence of the hard ceramic ZrO_2 skin provides essential resistance against superficial scratching and fretting wear, which are critical precursors to cladding failure [16].

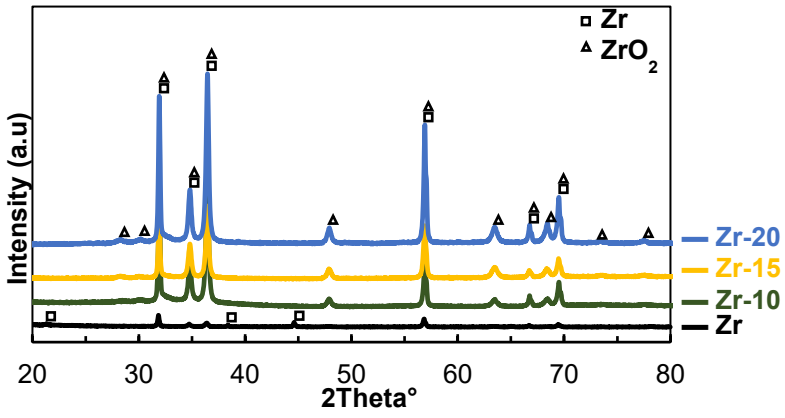

Figure 5. XRD pattern of zirconium oxide (ZrO_2)

 DOI: https://doi.org/10.55981/urania.2026.15001

Table 2. Average and Standar Deviation (STDV) for Microhardness of Zr-Anodized under different duration process.

Specimen	HV					Average	Standard Deviation
	1	2	3	4	5		
Zr-10	150.97	138.23	140.08	158.57	134.19	144.41	8.99
Zr-15	156.89	142.93	138.07	149.92	135.5	144.66	7.84
Zr-20	155.79	144.39	137.77	136.86	139.61	142.88	6.96

An oxide layer thickness quantitative summary and cross-sectional SEM images of anodized zirconium specimens treated for 10, 15, and 20 minutes are shown in Table 3 and Figure 6. This figure aims to assess how anodization time affects the shape and growth behavior of the anodic oxide layer that forms on zirconium. From Zr-10 (3.30 ± 0.67 μm) to Zr-15 (4.72 ± 1.12 μm) and Zr-20 (6.96 ± 1.42 μm), the SEM micrographs show clearly a compact and rather homogeneous oxide layer adhering to the substrate. The oxide–metal contact is displayed by the dotted line, which highlights the continuous layer growth without significant delamination. A time-dependent oxide the growth process controlled by field-assisted ionic transport, where Zr^{+} cations migrate outward and O^{2-} anions migrate inside under a strong electric field to create ZrO_2 at the interface, is suggested by the increasing thickness with anodization time. High-field oxide growth theory states that unless transport limitations or dissolving effects become visible, oxide thickness is proportional to the applied potential and processing time.

Table 3. Oxide layer thickness of anodized zirconium specimens

Specimen	Thickness (μm)
Zr-10	3.30 ± 0.67
Zr-15	4.72 ± 1.12
Zr-20	6.96 ± 1.42

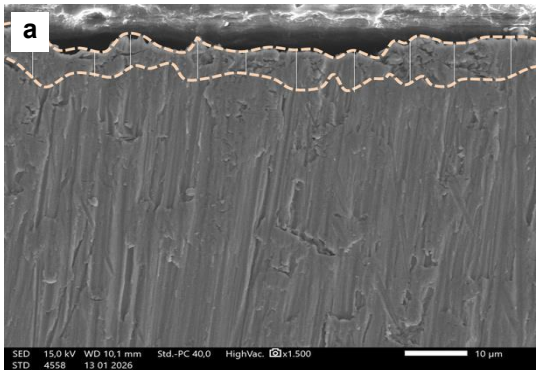

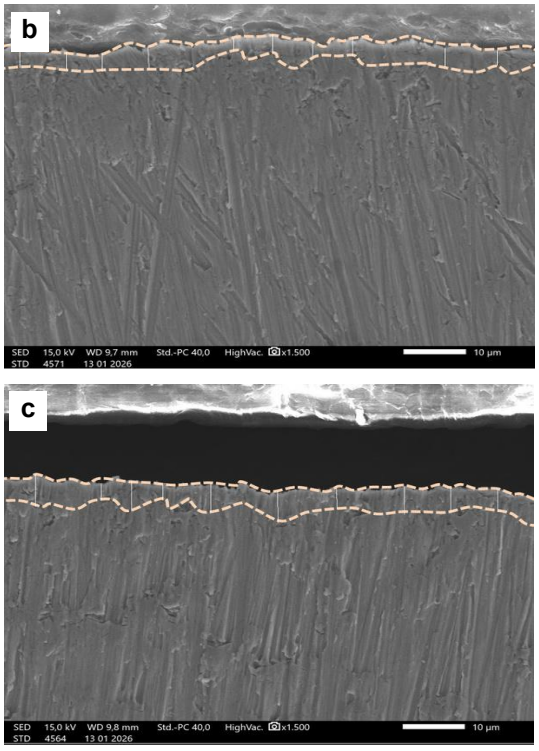

Figure 6. Cross-sectional view SEM images for zirconium anodized of (a) Zr-10, (b) Zr-15, (c) Zr-20 minutes.

Electrochemical Corrosion Behavior

The corrosion resistance was comprehensively analyzed using OCP, PDP, and EIS techniques. Open Circuit Potential (OCP): Figure 7 illustrates the OCP evolution. All anodized specimens exhibited more positive (noble) potentials compared to the bare substrate. The Zr-20 sample showed the most noble potential, stabilizing at a higher value, which indicates a thermodynamic tendency to resist spontaneous corrosion reactions in the electrolyte [17]. During the test, pure zirconium (Zr) specimens had the most negative and comparatively steady potential values, suggesting more potential for corrosion. All the specimens indicated a potential change in a more positive direction immediately after the anodization process,

which suggests that the formation of a zirconium oxide layer had increased electrochemical stability. Zr-20, Zr-15, and Zr-10 were the anodized specimens with the most positive and consistent OCP values while the test. This suggests that extending the anodization duration increases the material's resistance to corrosion and creates a more protective oxide layer. The formation of a rather stable passive layer on the zirconium surface is also shown by the stability of the OCP curves over an extended test time.

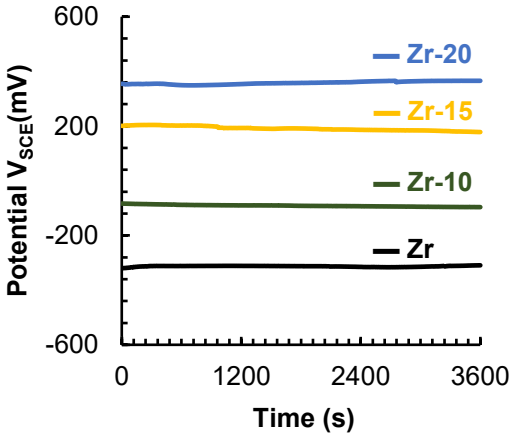

Figure 7. Average of OCP curves for zirconium substrate and zirconium-anodized at 30 V

Potentiodynamic Polarization (PDP): The Tafel polarization curves in Figure 8 demonstrate a clear shift in corrosion kinetics. The electrochemical parameters summarized in Table 4 show a dramatic reduction in corrosion current density (i_{corr}). The substrate exhibited an i_{corr} of 12.93 × 10^{-9}A/cm^2. In contrast, the Zr-20 specimen exhibited an i_{corr} of 0.19 × 10^{-9}A/cm^2. This reduction by nearly two orders of magnitude confirms that the thicker oxide layer formed at 20 minutes acts as an effective barrier, blocking the diffusion of chloride ions (Cl^-) and oxygen to the metal interface [18, 19].

Figure 8 presents the potentiodynamic polarization (PDP) curves of anodized and pure zirconium. These curves illustrate the relationship between the voltage across a reference electrode and the log current density, which is used to assess corrosion behavior and electrochemical reaction kinetics. Pure zirconium exhibits poor corrosion resistance, indicated by its limited passivation range and relatively high corrosion current density. In contrast, anodized specimens show a shift in corrosion potential to more positive values and a decrease in corrosion current density. Compared to Zr-15 and Zr-10, the Zr-20 specimen shows the biggest passivation area and the lowest current density. The Zr-20 specimen exhibits the lowest current density and the largest passivation region compared to Zr-15 and Zr-10. This suggests that the zirconium oxide layer that develops over extended anodization durations successfully prevents charge transfer and reduces the rate of corrosion.

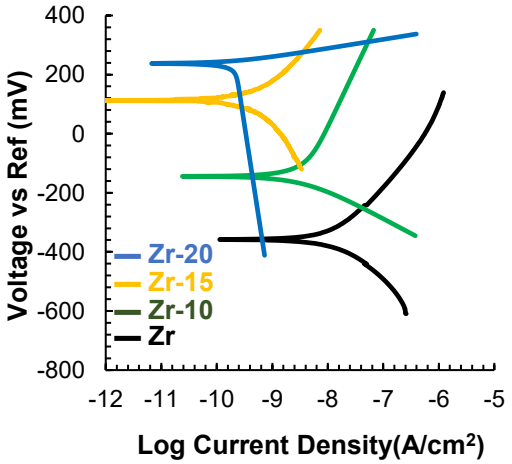

Figure 8. Average of PDP curves for zirconium substrate and zirconium-anodised at 30 V.

The blue curve corresponds to the Zr-20 specimen, which exhibits the longest anodizing duration (20 minutes). The distinct shape of this curve compared to the other samples is primarily attributed to differences in the oxide layer thickness, compactness, and electrochemical stability resulting from prolonged anodization. Several factors explain this behaviour, due to more Compact and Thicker Oxide Film. The Zr-20 sample forms a thicker and denser ZrO_2 layer, as supported by higher oxygen atomic percentage (EDS), lowest surface roughness (Ra = 0.24 μm), lowest corrosion current density (0.19 × 10^{-9} A/cm²). This compact oxide layer significantly suppresses charge transfer at the metal/electrolyte interface, resulting in:

A pronounced shift of Ecorr toward more positive values, a wider passive region, lower anodic current density. The shape

 DOI: https://doi.org/10.55981/urania.2026.15001

difference reflects a more stable passive regime in Zr-20. The reduced slope in the anodic branch indicates lower metal dissolution kinetics due to improved barrier characteristics of the oxide.

Shorter anodizing times (10 and 15 minutes) likely produce thinner films with higher defect density or localized porosity. These structural differences lead to earlier activation behavior and less stable passivation, resulting in PDP curves that differ in shape.

For Zr-20, corrosion behavior transitions from activation-controlled to diffusion-limited/passivation-controlled kinetics over a wider potential range, which explains the distinct curvature compared to the other samples.

Table 4. PDP Parameter of Zr-Anodized under different duration process.

Specimen	E_{corr} (mV)	i_{corr} (10^{-9}A/cm^2)	β_{Anodic} (mV/Decade)	$\beta_{Catodic}$ (mV/Decade)
Zr	-346 ± 88	12.93 ± 2.89	399 ± 350	275 ± 152
Zr-10	-114 ± 94	2.57 ± 1.12	599± 461	198 ± 122
Zr-15	92 ± 98	1.10 ± 0.82	275 ± 201	363 ± 262
Zr-20	233 ± 74	0.19 ± 0.04	152 ± 151	1518 ± 1067

Figure 9, the EIS results show that anodized samples exhibit significantly larger semicircle diameters in the Nyquist plots compared to the bare zirconium substrate, indicating improved corrosion resistance after anodization. The fitted parameters reveal that the charge transfer resistance (Rct) increases with anodizing time, with Zr-20 showing the highest resistance value, confirming enhanced barrier properties of the oxide layer. The solution resistance (Rs) remains relatively constant, suggesting consistent electrolyte conditions during testing. Additionally, the decrease in CPE values and the broader capacitive region in the phase angle plots indicate improved film compactness and reduced surface heterogeneity. Overall, the EIS analysis supports the PDP and OCP results, confirming that longer anodizing duration produces a thicker and more protective ZrO_2 layer that effectively suppresses corrosion reactions.

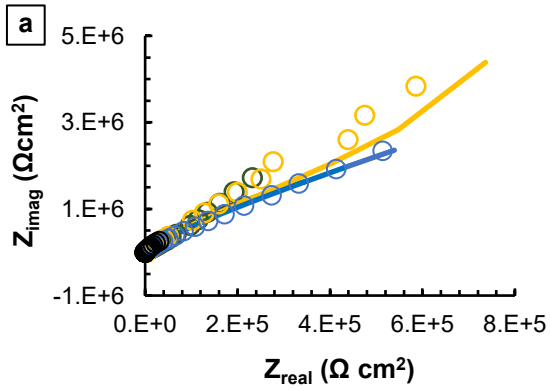

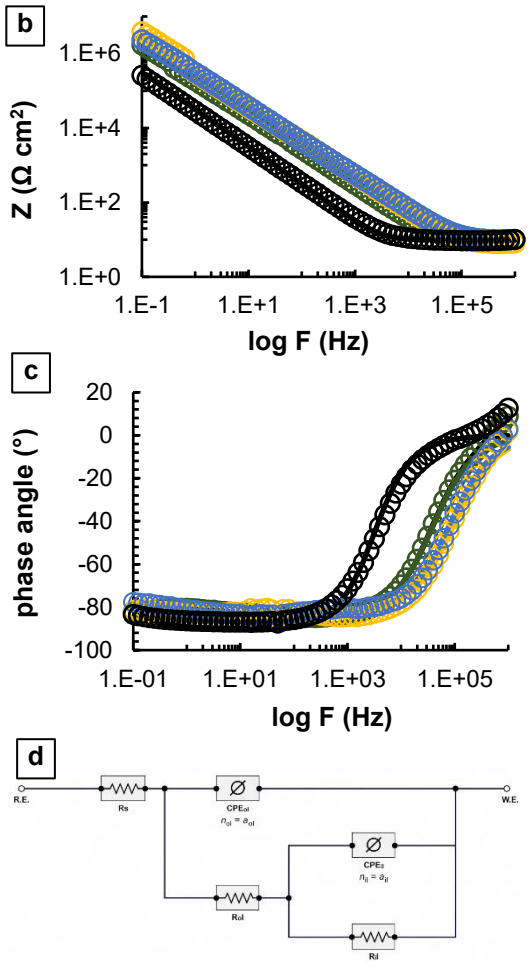

Figure 9. Average of EIS results of a) Nyquist spectra, b) bode impedance, c) bode phase, d) Equivalent electrical circuit (EEC) fitting for zirconium substrate and zirconium-anodised at 30 V.

Based on Table 5, the solution resistance (Rs) remains nearly constant at approximately 10–11 Ω·cm² for all samples, confirming stable electrolyte conditions. The oxide-related resistance and charge transfer resistance increase significantly after anodization, with Rct rising from 137 Ω·cm² for Zr-10 to 150 Ω·cm² for Zr-15 and reaching 140 Ω·cm² for Zr-20, indicating improved interfacial stability. The CPE values decrease slightly from 1×10^{-8} to 6.1×10^{-8} $S\cdot s^{n}\cdot cm^{-2}$ as anodizing time increases, suggesting a more compact and less defective oxide layer. The goodness-of-fit values (χ^2 in the order of 10^{-2}) indicate that the equivalent circuit model adequately represents the experimental data. These quantitative results confirm that increasing anodizing time increases the electrochemical resistance of the zirconium surface.

Table 5. Fit parameters of EIS data.

Parameter	Substrate	Zr-10	Zr-15	Zr-20
R_s ($\Omega.cm^2$)	10	11	159	10
C_{dl} ($S^*s^a.cm^{-2}$)	$5x10^{-6}$	-	-	-
R_{ct} (Ω:cm^2)	$2x0^6$	-	-	-
CPE_{ol} ($S^*s^a.cm^{-2}$)	-	$1x10^{-8}$	$8x10^{-8}$	$6.1x10^{-8}$
a_{ol}	-	0.6	0.7	0.7
R_{ol} ($\Omega.cm^2$)	-	137	150	140
CPE_{il} ($S^*s^a.cm^{-2}$)	-	$9.3x10^{-9}$ 10^{-9}	$5.6x10^{-9}$ 10^{-9}	$5.3x10^{-9}$ 10^{-9}
a_{il}	-	0.9 10^{-3}	0.9 10^{-3}	0.9 10^{-3}
R_{il} ($\Omega.cm^2$)	-	15.00 106	15.82 106	16.40 103
Goodness of fit (χ^2)	$1.1x10^{-2}$	$3.4x10^{-2}$	$2.3x10^{-2}$	$1.4x10^{-2}$

CONCLUSIONS

The effect of anodizing duration on the surface characteristics and corrosion behavior of Zirconium was successfully investigated. The following conclusions are drawn:

1. Surface Improvement: Increasing the anodizing time from 10 to 20 minutes at 30 V results in a progressively smoother surface. The Zr-20 specimen achieved the lowest roughness (Ra= 0.24 μm), reducing friction and potential pit initiation sites.
2. Oxide Formation: The process forms a stable, crystalline ZrO_2 layer, as confirmed by XRD and the observation of interference colors.
3. Corrosion Resistance: The 20-minute anodized coating offers superior corrosion protection in chloride environments. It reduced the corrosion rate i_{corr} by approximately 98% compared to the bare substrate and significantly increased the polarization resistance.
4. Application Viability: The study confirms that a 20-minute anodizing treatment is an effective, low-cost method to enhance the durability of Zirconium nuclear fuel cladding, potentially extending the safety margins against corrosion and mechanical degradation in PWR environments.

ACKNOWLEDGEMENT

We would like to thank our gratitude to the Universitas Kristen Indonesia (UKI) through the UKI Institute for Research and Community Service (LPPM) for funding this research.

REFERENCES

[1]. A. T. Motta, A. Couet, and R. J. Comstock, “Corrosion of zirconium alloys used for nuclear fuel cladding,” *Annual Review of Materials Research*, vol. 45, pp. 311–343, 2015.

[2]. Z. Duan, H. Yang, Y. Satoh, and K. Murakami, “Oxidation behavior of zirconium alloys in a simulated nuclear reactor primary coolant,” *Journal of Nuclear Materials*, vol. 485, pp. 147–158, 2017.

[3]. K. A. Terrani, “Accident tolerant fuel cladding development: Promise, status,

and challenges," *Journal of Nuclear Materials*, vol. 501, pp. 13–30, 2018.
[4]. W. Gong and D. Yun, "A review on the corrosion behavior of zirconium alloys in supercritical water," *Corrosion Science*, vol. 208, p. 110620, 2022.
[5]. A. Yilmazbayhan, A. T. Motta, and R. J. Comstock, "Hydride morphology and embrittlement in Zircaloy-4 cladding," *Journal of Nuclear Materials*, vol. 545, p. 152646, 2021.
[6]. J. Liu and Q. Li, "Fretting wear behavior of zirconium alloy cladding tubes," *Wear*, vol. 522, p. 204689, 2023.
[7]. H. G. Kim and I. H. Kim, "Oxidation behavior of zirconium alloy claddings in high temperature steam," *Nuclear Engineering and Technology*, vol. 52, no. 4, pp. 808–815, 2020.
[8]. S. Suresh and A. Sharma, "Surface modification of zirconium alloys for biomedical and nuclear applications: A review," *Surface and Coatings Technology*, vol. 405, p. 126666, 2021.
[9]. R. Verma and S. Kumar, "Electrochemical anodization of zirconium: Growth mechanism and properties," *Electrochimica Acta*, vol. 412, p. 140135, 2022.
[10]. Y. Cheng and E. Matykina, "Formation of nanotubular oxide layers on zirconium alloys by anodization," *Corrosion Science*, vol. 182, p. 109289, 2021.
[11]. F. Ali and M. Al-Hajri, "Effect of voltage and electrolyte composition on the morphology of anodic zirconium oxide," *Materials Chemistry and Physics*, vol. 295, p. 127087, 2023.
[12]. L. Wang, Y. Zhang, and X. Wu, "Time-dependent growth kinetics of anodic films on zirconium in phosphate electrolytes," *Journal of Electrochemical Society*, vol. 171, no. 2, p. 021504, 2024.
[13]. M. V. Diamanti and M. P. Pedeferri, "Color production on zirconium by anodizing: Interference and absorption effects," *Color Research & Application*, vol. 45, no. 3, pp. 456–464, 2020.
[14]. G. E. Thompson, "Porous anodic oxide films: Formation, growth and applications," *Thin Solid Films*, vol. 685, pp. 34–45, 2019.
[15]. X. Zhao and H. Xu, "Phase transformation in anodic zirconia films: From amorphous to crystalline," *Scripta Materialia*, vol. 210, p. 114421, 2022.
[16]. E. G. Obbard and P. A. Burr, "Mechanical properties of zirconium oxide scales: A review," *Journal of Nuclear Materials*, vol. 557, p. 153255, 2021.
[17]. E. McCafferty, Introduction to Corrosion Science, 2nd ed. Springer, 2020.
[18]. B. Zhang and G. S. Frankel, "Corrosion mechanisms of zirconium alloys in chloride-containing environments," *Corrosion*, vol. 78, no. 5, pp. 412–425, 2022.
[19]. T. Li and F. Wang, "Improvement of pitting corrosion resistance of Zr alloys by anodic oxidation," *Applied Surface Science,* vol. 610, p. 155567, 2023.
[20]. M. E. Orazem and B. Tribollet, Electrochemical Impedance Spectroscopy. Wiley, 2017.